Research Square

Preprints are preliminary reports that have not undergone peer review.
They should not be considered conclusive, used to inform clinical practice,
or referenced by the media as validated information.

The Discovery of Thirteen Hydrothermal Vent Fields and associated Polymetallic Massive Sulfides in the Central Indian Ocean

Sebastian Fuchs
sebastian.fuchs@bgr.de

Federal Institute for Geosciences and Natural Resources (BGR) Germany
Thomas Kuhn
Federal Institute for Geosciences and Natural Resources (BGR) Germany
Klaas Meyn
Federal Institute for Geosciences and Natural Resources (BGR) Germany
Terue Kihara
INES – Integrated Environmental Solutions GmbH
Dieter Garbe-Schönberg
Kiel University
Meike Klischies
Ocean.Data.Rocks
Ralf Freitag
Federal Institute for Geosciences and Natural Resources (BGR) Germany
Ulrich Schwarz-Schampera
Federal Institute for Geosciences and Natural Resources (BGR) Germany

Article

Keywords: Polymetallic seafloor massive sulfides deposits, deep-sea mineral exploration, black smoker, hydrothermal vents, base and precious metal mineralization, faunal vent communities

Posted Date: May 26th, 2026

DOI: https://doi.org/10.21203/rs.3.rs-9695993/v1

License: This work is licensed under a Creative Commons Attribution 4.0 International License. Read Full License

Additional Declarations: No competing interests reported.

Abstract

We report the discovery and first integrated characterization of thirteen previously unknown hydrothermal vent fields and associated seafloor massive sulfide occurrences within an exploration contract area around the Rodrigues Triple Junction, spanning the southern Central Indian Ridge and northern Southeast Indian Ridge. The newly identified fields—Alpha, Gauss, Score, Kaimana, Pelagia, Surya, Sooraj, Jim, New Sonne, Huna, Penumbra, Lux, and Umbra—include the first confirmed vent systems on the Southeast Indian Ridge. Vent sites were identified by systematic seafloor surveys, confirmed by remotely operated vehicle-based ground-truthing, and sampled. These vent fields occur in four tectonic settings—axial valley, ridge flank, off-axis volcanic plateau, and non-transform offsets—indicating that hydrothermal circulation and SMS formation are controlled by magmatic heat supply, fault-controlled permeability, crustal age, and local lithology. Vent fluids range from low-temperature diffuse discharge to supercritical, metal-rich brines and low-chloride, metal-poor vapor-type fluids; surface mineralization spans high-temperature sulfide assemblages, peripheral facies, silica-rich deposits, and oxidized inactive mounds. Megafaunal communities are dominated by typical Indian Ocean vent taxa and show zonation related to venting intensity and site activity. This study provides a baseline dataset for future geological, resource-related, biological, and environmental assessments.

1 Introduction

Polymetallic seafloor massive sulfides (SMS) are mineral accumulations formed by hydrothermal activity on the ocean floor, typically at mid-ocean ridges, volcanic arcs, and in back-arc basins. Since the first discovery of a hydrothermal vent field at the Galápagos Spreading Center[1], hydrothermal systems and their associated faunal communities have received increasing scientific attention, particularly in the Pacific and Atlantic oceans. To date, more than 720 hydrothermal vent fields and associated SMS occurrences have been documented worldwide[2]. These occurrences are commonly regarded as modern analogues of volcanic-hosted massive sulfide (VMS) deposits, which are mined on land and have represented important sources of base and precious metals throughout Earth history.

Seafloor massive sulfide occurrences may contain elevated concentrations of Cu, Zn, Fe, Pb, Au, and Ag, together with a variable suite of trace metals relevant to modern industrial applications. This metal association has made SMS occurrences important targets of marine mineral exploration, particularly in areas beyond national jurisdiction. At the same time, their potential contribution to future metal supply remains uncertain, because most occurrences are still poorly constrained in terms of size, grade, continuity, and subsurface extent, and because any future exploitation would have to address substantial technological, regulatory, and environmental challenges. Consequently, SMS exploration provides not only information relevant to resource assessment, but also unique baseline datasets for understanding hydrothermal circulation, metal transport and deposition, chemosynthetic ecosystems, and the environmental sensitivity of deep-sea habitats.

The International Seabed Authority (ISA) issues contracts for the exploration of SMS in international waters outside national jurisdiction, referred to as the Area, in accordance with the United Nations Convention on the Law of the Sea (UNCLOS). Hydrothermal activity in the Indian Ocean has been investigated since the 1980s, when water-column anomalies and early geochemical surveys provided the first evidence for hydrothermal discharge near the Rodrigues Triple Junction and along adjacent ridge segments. Subsequent ROV-based discoveries of the Kairei and Edmond vent fields established the Central Indian Ridge as a key region for hydrothermal research. Since then, systematic geophysical, geochemical, and ROV-based surveys have progressively expanded the known distribution of hydrothermal vent fields and associated SMS occurrences in the Indian Ocean. Currently, 20 active hydrothermal vent fields in the Indian Ocean have been confirmed by video imagery and studied or sampled to varying degrees.

Along the Carlsberg Ridge (CR), five vent fields have been documented: Wocan-1 and Wocan-2[3,4], Daxi[5], Tianxiu[6], and Tianshi[7]. Along the Central Indian Ridge (CIR), eleven vent fields have been reported: Onnuri[8], Onnarae, Mirae, Ari, Cheoeum, Onbada, Tamaki, Dodo[9], Solitaire[10], Sonne, Edmond[11], and Kairei[11,12]. Among these, Kairei and Edmond are historically important because they were the first two active hydrothermal vent fields discovered and confirmed in the Indian Ocean. Kairei was discovered in 2000 near the Rodrigues Triple Junction during a Japanese expedition with R/V Kairei and ROV Kaiko was the first active hydrothermal vent field discovered in the Indian Ocean. It was found during a Japanese research expedition using R/V Kairei and the remotely operated vehicle (ROV) *Kaiko* near the Rodrigues Triple Junction[12,13]. Edmond was identified in 2001 during an expedition with R/V Knorr and ROV Jason, although water-column anomalies had already indicated hydrothermal activity in this region in the late 1980s[11,14,15]. Along the Southwest Indian Ridge (SWIR), the Longqi[16-18], Duanqiao[18], and Tiancheng[16,18] vent fields have been described. In contrast, hydrothermal activity along the Southeast Indian Ridge (SEIR) has remained poorly documented, with only Site 21[19] reported until recently.

The Federal Institute for Geosciences and Natural Resources (BGR), Germany, began prospecting for SMS occurrences in the central Indian Ocean in 2011, leading to an ISA exploration contract for polymetallic sulfides on 6 May 2015 (Figure 1). Under this 15-year contract, BGR has conducted ten research expeditions to the contract area. Fifteen vent fields have been localized within the contract area to date, including the previously known Kairei and Edmond fields. As a result of these exploration campaigns, 13 previously unknown vent fields and associated SMS occurrences were discovered along the southern CIR and northern SEIR, including the first confirmed vent fields on the SEIR (Figure 1). Here, we present the first integrated characterization of these new discoveries, including their geological and tectonic setting, seafloor morphology, sulfide mineralogy, host-rock associations, hydrothermal fluid chemistry, and megafaunal communities. This study provides a baseline dataset for future geological, geochemical, biological, environmental, and resource-related assessments of hydrothermal systems and SMS occurrences in the central Indian Ocean.

2 Geological and tectonic settings

The identified vent fields and associated SMS occurrences can be grouped into four categories according to their bathymetric position and related tectonic setting: (i) axial valley group, (ii) ridge-flank group, (iii) off-axis volcanic-plateau group, and (iv) non-transform-offset group (Figure 2; Table 1; STable 1). The first group, the axial valley group, comprises the Pelagia and New Sonne vent fields. Both are located on young oceanic crust (<100,000 years) in the SEIR

central valley, where Pelagia rests on an axial volcanic ridge and New Sonne on the first valley flank. This setting is typical of many mid-ocean ridges[20]. At such sites, hydrothermal convection is driven by local, spreading-related magmatic activity and the formation of new oceanic crust. Hydrothermal fluids commonly circulate through active fissures and faults generated by magmatic rifting[20].

The second group, the ridge-flank group, comprises the vent fields Surya, Edmond, Gauss, Score, Kaimana, and Kairei. They occur on older ridge flanks at greater distances from the central valley, with Surya located approximately 6 km off the ridge axis, Kairei approximately 8 km, and Kaimana approximately 10 km. Edmond, Gauss, and Score cluster at a distance of approximately 4 km from the CIR axis. Assuming constant spreading rates for the CIR[21], these distances correspond to estimated crustal ages of ca. 150,000 years for Edmond, Gauss, and Score to ca. 430,000 years for Kaimana.

The third group comprises vent fields associated with an off-axis volcanic plateau, including Huna, Penumbra, Lux, and Umbra. These fields are located 12–17 km east of the SEIR spreading axis (Figure 1), where the seafloor forms an elevated morphology. SMS mineralization is aligned along larger ridge-parallel normal faults or occurs within a tectonic graben on the volcanic plateau. The crustal segment shows estimated spreading ages between 460,000 and 650,000 years[21]. The plateau morphology, together with a distinct positive Bouguer anomaly in ship-based gravimetric data (unpublished BGR data), may indicate mantle upwelling or anomalously elevated heat flow beneath this part of the SEIR flank. Such an additional heat source could explain hydrothermal convection at these distances from the active spreading center.

The Alpha, Sooraj, and Jim vent fields form a distinct fourth group associated with SMS occurrences located along non-transform offsets. These occurrences lie within or close to active ridge offsets, where the surrounding seafloor displays complex structural patterns and exposes deeper crustal rocks and upper mantle material. This tectonically complex setting prevents the estimation of distinct crustal ages. However, the presence of basaltic rocks in or near some of these fields indicates that magmatic activity may also contribute to, or locally drive, hydrothermal convection.

3 General geological characteristics of the discovered vent fields

3.1 Introduction

Four of the newly discovered vent fields are located on the southern Central Indian Ridge (CIR) and nine on the northern Southeast Indian Ridge (Fig. 1). They are named Alpha, Gauss, Score, Kaimana, Surya, Sooraj, Pelagia, Jim, New Sonne, Huna, Penumbra, Lux, and Umbra. An overview of these fields, including their approximate positions, water depths, areal extent, and years of discovery, is presented in Table 1, with further details provided in Supplemental Table 1. All vent fields within the BGR contract area, including the previously known Edmond and Kairei fields, occur at water depths between 2,375 and 3,660 m. Typical characteristics of the SMS occurrences are shown in Fig. 3 and in more detail in Supplemental Figs. 1–12.

The vent fields discovered along the CIR and SEIR consist of one or several hydrothermal sites. These sites include actively venting black smoker chimney complexes, inactive chimney complexes representing former high-temperature discharge, hydrothermal mounds with or without chimney structures, isolated sulfide chimneys aligned along open fissures, and areas of hydrothermally stained sediment locally covered by bacterial mats or hydrothermal fauna. Where several sites occur within a single vent field, they may be separated by background seafloor lithologies, such as basaltic lava flows, talus, or pelagic sediment cover. Individual sites within a field are typically spaced tens to several hundreds of meters apart. By contrast, separate vent fields are interpreted to reflect distinct hydrothermal circulation systems and are commonly separated by several to several tens of kilometers. However, some of the SMS occurrences identified here as separate vent fields may ultimately belong to larger, structurally connected hydrothermal systems.

We distinguish between active and inactive hydrothermal sites based on the presence or absence of visible high-temperature or diffuse low-temperature venting at the time of observation. This operational distinction is used for descriptive purposes, while acknowledging that the transition between active, inactive, and extinct systems is more complex and may vary over time[22].

3.2 Active vent fields and associated SMS occurrences

Active vent fields comprise one or more geologically distinct vent sites, which may include both active and inactive components. Most active fields are hosted by basaltic rocks. Exceptions include Kaimana, Sooraj, and Jim, which are associated with exhumed deeper oceanic crust and upper mantle lithologies. Observed rock types include gabbroic rocks and variably serpentinized peridotites, mainly harzburgite and lherzolite, with subordinate pyroxenite and dunite. Although Alpha and Kairei are surrounded by basaltic rocks at the seafloor, fluid chemical and geological evidence suggests that deeper plutonic to ultramafic lithologies may contribute to their hydrothermal systems. The associated SMS occurrences are mainly characterized by hydrothermal mounds on the seafloor, ranging from small, low-relief mounds to larger edifices up to approximately 200 m in basal diameter and 50 m in height. Individual mounds cover areas from about 1,950 m² at Surya to 75,535 m² at the active Kairei site. Mineralization also includes scattered inactive chimney blocks and rafts, sulfide talus, hydrothermally stained sediments, and hydrothermal crusts. Specific characteristics of selected SMS occurrences are described below.

The active vent fields Alpha, Edmond, Kaimana, Jim, Penumbra, and Huna contain at least one large chimney complex, locally reaching heights of up to 30 m (Fig. 3A, C; SFigures 1A, 2A, 7A, 10A, B). These complexes consist of several chimney spires discharging high-temperature hydrothermal fluids with measured temperatures between 296°C at Jim and Huna and 418°C at Edmond. The active chimney complexes commonly occur on top of steep-sided, conical, or terraced breccia mounds (Fig. 3A; SFigures 1B, 2B, C, 3A, C, E, F, 4B, E, 7C, 8A, D). They are surrounded by more gently sloping mound margins covered by ferruginous sediment and scattered sulfide blocks. Flatter terrace surfaces may be covered by Fe-oxide hydrothermal crusts and unconsolidated reddish-brown, ferruginous, or grey hydrothermal sediment (Fig. 3D, E; SFigures 1E, 3B, F, 5C, 6F, 7C, 8C, D, 10D–F). Steeper mound flanks and mound crests are commonly characterized by red-brown ferruginous sediment, patchy hydrothermal crusts, variably oxidized sulfide blocks, and chimney debris. The abundance of sulfide breccia generally increases toward mound crests and in proximity to active or inactive chimneys. Chimneys are commonly aligned

parallel to the long axis of the mound, and mound morphologies range from nearly circular to elongated. Prominent examples occur at Penumbra sites 6 and 12, Huna sites 1 to 5, New Sonne sites 1, 3, and 4, Kaimana site 1, the active Surya mound, and the active mound at Kairei.

The active Huna hydrothermal field differs from most sulfide-dominated systems described in this study. A distinguishing feature is the presence of silica-rich mounds and silica patches developed on basaltic talus. These deposits are composed mainly of loose, fine-grained silica precipitates. Silica precipitates from clear, high-temperature fluids that discharge through small silica micro-smokers and diffusely through surrounding mound surfaces and flanks (Fig. 3G; SFigure 9A–E). Morphologically, the silica mounds resemble crusted sulfide mounds, but they display characteristically smooth, rounded upper surfaces. They are commonly tiered, with flanks dipping at approximately 40° and relatively flat summits. Their surface material consists of coarse sand- to pebble-sized hydrothermal sediment. The upper mound surfaces and flanks contain irregular crust-like silica blocks with botryoidal surfaces, typical of silica sinter. Fragments of sulfide chimneys are locally observed at the base of the mounds and are interpreted as earlier sulfide precipitates that predate silica sinter formation (SFigure 9E). In addition, tower-like silica shelf structures up to approximately 30 m high occur in the vicinity of the Huna field, but not directly at the active vents. These silica shelves consist of solid silica with fine-grained intercalated iron oxyhydroxides, such as goethite, giving them a yellowish coloration. Their surfaces are commonly covered by thick Fe–Mn crusts (SFigure 9G, H).

The Sooraj vent field contains one central hydrothermal mound with active black smoker chimneys. With a basal diameter of only a few tens of meters and a height of a few meters, this mound is comparatively small relative to the larger mound complexes observed at other SMS occurrences. Approximately 200 m southwest of the central active mound, diffuse fluid discharge forms low-relief hydrothermal areas with scattered small chimneys, hydrothermal sediments, and crusts. In contrast, older inactive chimneys are aligned along open fissures over a strike length of approximately 500 m in the northeastern part of the Sooraj field (Figs. 3E and 5; SFigure 5A, B, E). These chimneys are small, upright, mostly intact, and range from approximately 5 cm to 5 m in height.

3.3 Inactive vent fields and non-venting SMS occurrences

In the absence of visible hydrothermal venting, inactive SMS occurrences are characterized by relict chimney structures, sulfide talus, hydrothermally stained sediments, hydrothermal crusts, and crusted mounds. Crusted mounds are a dominant feature of many inactive sites. They may be terraced or non-terraced and generally display gentler slopes than sulfide breccia mounds associated with active chimney complexes. Their surfaces are commonly covered by centimeter- to meter-scale hydrothermal crusts composed of Fe-oxides and hydrothermal silica, with only scattered sulfide blocks exposed at the surface. Small pits, typically 1–3 m in diameter and up to approximately 1 m deep, occur on the tops of some mounds, for example at Penumbra site 5. Light yellowish-brown veins filled with iron oxyhydroxides and old mini-chimneys are also observed locally. The gently sloping margins of crusted mounds are broadly similar to those of sulfide breccia mounds, but commonly display a more continuous hydrothermal crust cover.

Examples of crusted sulfide mounds include inactive sites 1–5, 9, and 10 within the active Jim field, and inactive sites 1, 4, 5, and 7 at Penumbra. Most sites in the inactive SMS occurrences at Lux, Gauss, and Score also form crusted mounds. Typical characteristics of inactive fields are shown in Fig. 3B and H and in more detail in Supplemental Figs. 2, 11, and 12.

Oxidized stringer-style sulfide mineralization is observed at several sites where mineralized footwall or stockwork zones appear to have been exposed by syn- to post-mineralization faulting, mass wasting, or erosion. Examples occur at Surya, Sooraj, and New Sonne. At Surya, oxidized stringer-style mineralization is exposed within a mound composed of sulfide and pillow basalt talus (Fig. 3D; SFigure 4E, F). It remains uncertain whether these exposures represent larger blocks derived from an altered and mineralized footwall zone, or whether they are in situ exposures of underlying stringer mineralization surrounded by sulfide and basalt talus. Similar mineralization is observed at Sooraj and New Sonne (Fig. 3F; SFigure 8D, G). These occurrences may represent modern analogues of stockwork or stringer zones observed beneath ancient VMS deposits[23, 24].

4 Hydrothermal fluids and associated SMS mineralization

4.1 Hydrothermal Fluids

Hydrothermal vent fluids from the INDEX area show large variations in temperature, pH, salinity, chloride concentration, and dissolved metal contents, reflecting diverse physicochemical conditions along the southern Central Indian Ridge and northern Southeast Indian Ridge. Measured vent-fluid temperatures range from diffuse discharge of about 31°C at Surya to supercritical venting of 418°C at Edmond, whereas salinities vary from 0.9 wt.% NaCl at Huna to 4.9 wt.% NaCl at Edmond. The measured pH_{25} values range from 3.2 to 6.5 (STable 1). In a bivariate plot of chloride versus summed dissolved metals, the sampled fluids define two broad compositional groups: Cl- and metal-rich brine-type fluids and Cl- and metal-poor vapor-type fluids (SFigure 13). This distribution indicates substantial phase separation and subsequent fluid modification within the INDEX hydrothermal systems.

Brine-type fluids were sampled at Alpha, Edmond, Kairei, Kaimana, and Sooraj. These fluids are characterized by elevated chloride concentrations, reaching up to approximately 1.7 times seawater values, high dissolved metal contents, and acidic to moderately acidic pH_{25} values. The most saline endmembers occur at Edmond, Alpha, and Kaimana, with NaCl concentrations of 3.6–4.9 wt.% and pH_{25} values of 3.2–3.6. These fluids carry high concentrations of dissolved Fe, Cu, and Zn and, where measured, elevated dissolved H_2S, consistent with high-temperature leaching of basaltic to deeper crustal rocks and preferential metal partitioning into the dense saline phase during phase separation[25, 26]. Total dissolved metal concentrations in these fluids reach several millimoles per kilogram, with Fe + Mn + Cu + Zn locally reaching approximately 3–15 mmol/kg, corresponding to metal loads of several hundred mg/kg fluid and overlapping with values reported from metal-rich black smoker systems worldwide[27, 28] (SFigure 13). Edmond, with measured vent-fluid temperatures of up to 418°C, represents one of the hottest hydrothermal systems reported from a mid-ocean-ridge setting and records supercritical discharge conditions.

Vapor-type fluids were sampled at New Sonne, Jim, Huna, and Penumbra. These fluids are characterized by lower chloride concentrations and lower summed dissolved metal contents relative to the brine-type fluids. They have comparatively low salinities, particularly at Huna, Penumbra, and New Sonne, and pH_{25}

values between 4.1 and 5.5. Their metal-poor character is consistent with phase separation, during which many metals preferentially partition into the saline brine phase, leaving the coexisting vapor-derived fluid depleted in metals[29]. The silica-rich mineralization at Huna is consistent with discharge of low-salinity, vapor-type fluids at temperatures up to 296°C, comparable to phase-separation-related processes previously described from Indian Ocean vent systems such as Kairei and Edmond[30].

The INDEX fluid compositions therefore record a continuum between saline, metal-rich brine-type fluids and low-Cl, metal-poor vapor-type fluids rather than strictly discrete endmember classes. Some vent fields illustrate this complexity: Sooraj plots with the brine-type fluids in terms of Cl and metal contents, whereas Jim plots with the vapor-type group despite evidence for high-temperature hydrothermal circulation. Low-temperature diffuse discharge at Surya represents an additional modified-seawater component. Such variability indicates that phase separation, conductive cooling, fluid–rock interaction, subseafloor mixing, and permeability structure all influence the final composition of fluids discharged at the seafloor.

Overall, the INDEX vent fluids span a broad thermal and chemical range typical of mid-ocean-ridge hydrothermal systems, from dense, saline, metal-rich black smoker fluids to low-Cl, metal-poor vapor-type fluids and diffuse modified seawater. This variability reflects the combined effects of temperature, pressure, phase separation, host-rock interaction, and permeability structure on hydrothermal circulation and fluid evolution[27, 29, 31].

4.2 Mineralogy

The mineralogical composition of the massive sulfide occurrences from the INDEX area reflects the broad range of hydrothermal fluid conditions observed along the southern Central Indian Ridge and northern Southeast Indian Ridge. Sulfide assemblages are dominated by chalcopyrite, pyrite/marcasite, and sphalerite, whereas galena occurs widely across the investigated fields but is volumetrically subordinate. Minor sulfide phases include bornite and covellite, whereas secondary Fe-oxyhydroxides (FeOOH) occur in oxidized material (STable 1). Isocubanite occurs locally in high-temperature assemblages, particularly at the Edmond, Kaimana, and Kairei vent fields. Non-sulfide phases include silica and anhydrite, with local occurrences of barite and atacamite. Native gold occurs only in trace amounts and has been observed in both high-temperature Cu–Fe assemblages and Zn-bearing assemblages, as well as in oxidized sulfide-rich sediments. Native copper, in contrast, is restricted to oxidized sediments.

The observed assemblages define the typical mineralogical continuum of seafloor massive sulfide systems, ranging from high-temperature Cu–Fe-rich chimney assemblages to lower-temperature Zn- and silica-bearing assemblages with minor Pb phases, and finally to late-stage oxidized mound surfaces. Chalcopyrite-rich assemblages occur preferentially in high-temperature vent structures and focused discharge zones, whereas sphalerite- and silica-bearing assemblages are more common in cooler peripheral, waning-stage, or subseafloor-influenced hydrothermal environments. Isocubanite–chalcopyrite–pyrite associations mark the highest-temperature stages of venting and are consistent with reduced, metal-rich fluids. In contrast, silica-rich precipitates and Fe-oxyhydroxide crusts with minor residual sulfides reflect lower-temperature discharge, diffuse flow, or post-venting oxidation. The silica-rich mineralization at Huna is particularly notable and is consistent with precipitation from vapor-influenced, low-salinity fluids at temperatures up to 296°C, broadly comparable to phase-separation-related processes previously described from Indian Ocean vent systems such as Kairei and Edmond.

No systematic mineralogical differences can presently be resolved between the different tectonic settings identified in this study. Instead, the INDEX samples indicate that the same principal SMS-forming processes operate across axial valley, ridge-flank, off-axis volcanic-plateau, and non-transform-offset environments. The significance of these settings is therefore expressed less in fundamentally distinct mineral assemblages than in the relative abundance, preservation state, and spatial distribution of mineral facies. Active chimney complexes preserve fresh Cu–Fe-rich high-temperature assemblages, whereas inactive mounds and relict hydrothermal sites are commonly characterized by oxidized Fe-oxyhydroxide- and silica-rich crusts, locally associated with atacamite, native copper, and residual sulfide material. Thus, the mineralogy demonstrates that comparable hydrothermal processes are repeated across different structural environments, with local variations controlled by fluid composition, permeability, host-rock interaction, and the stage of hydrothermal activity.

4.3 Geochemistry

More than 500 surface samples from the SMS occurrences were analyzed for bulk-rock geochemistry, representing one of the most extensive geochemical datasets currently available from the Central and Southeast Indian Ridges. The samples are dominated by Fe–Cu–Zn sulfide compositions typical of mid-ocean-ridge seafloor massive sulfide systems, with variable proportions of chalcopyrite-, pyrite/marcasite-, and sphalerite-rich material. A pronounced inverse relationship between Cu and Zn is observed across the dataset, consistent with the mineralogical zonation described above and reflecting variable proportions of chalcopyrite- and sphalerite-rich assemblages.

The bulk compositions broadly overlap with published global mid-ocean-ridge SMS datasets[32, 33] (SFigure 14). Their internal variability likely reflects local differences in host-rock lithology, fluid pathways, and hydrothermal evolution, consistent with established controls on seafloor hydrothermal mineralization[34]. The different host-rock associations described above provide an important geological context for fluid–rock interaction and metal mobilization. However, the available surface-sample geochemistry does not define a simple diagnostic trace-element signature for the mafic–ultramafic-influenced systems. Bulk-rock variability instead reflects the combined effects of host-rock association, mineralogical facies, fluid composition, temperature, redox conditions, and sulfide precipitation processes. Trace-element distributions show systematic relationships with the dominant sulfide assemblages. Copper is primarily associated with chalcopyrite- and isocubanite-bearing high-temperature assemblages. Gold concentrations are generally low but occur in both Cu-rich and Zn-bearing sample groups, indicating that Au is not restricted to a single sulfide facies. Silver is mainly associated with Zn-dominant mineralization and probably occurs in sphalerite and subordinate sulfosalt inclusions. Lead is a minor constituent overall and is mainly hosted by volumetrically subordinate galena in Zn- and silica-bearing assemblages. These relationships are consistent with the mineralogical observations and indicate that much of the trace-element variability is governed by the relative abundance of the main sulfide phases and by the thermal gradient from focused high-temperature venting to cooler peripheral mineralization and oxidation.

Overall, the geochemical characteristics of the INDEX SMS occurrences are consistent with global trends in mid-ocean-ridge seafloor massive sulfides. The new dataset does not define fundamentally new mineralization types. Instead, it demonstrates that the compositional range of mid-ocean ridge (MOR)-related SMS mineralization is developed across a variety of axial, off-axis, and structurally controlled environments along the southern Central Indian Ridge and northern Southeast Indian Ridge.

5 Vent communities

The faunal characterization of the hydrothermal vent fields discussed in this paper shows similarities among the newly discovered fields and with known vent fields from the CR, CIR, SWIR, and SEIR. Therefore, we provide a general description of the megafauna; specific characteristics of individual vent fields are presented separately in STable 2–7.

Active sites within the investigated vent fields are dominated by the alvinocaridid shrimp *Rimicaris kairei* Watabe & Hashimoto, 2002 (Fig. 4A + B), which commonly covers entire chimneys or swarms around vent orifices, forming areas with abundant exuviae deposits. Other decapods, including the shrimps *Mirocaris indica* Komai, Martin, Zala, Tsuchida & Hashimoto, 2006 and *Alvinocaris solitaire* Yahagi, Watanabe, Kojima & Beedesse, 2014, as well as the crab *Austinograea rodriguezensis* Tsuchida & Hashimoto, 2002 (Fig. 4D), were also observed. At the periphery of the vents, the stalked barnacle *Neolepas marisindica*[19] (Fig. 4C) is much more common than the balanomorph barnacle *Eochionelasmus sp*., with *N. marisindica* occurring in dense aggregations at Alpha, Kairei, Sooraj, Pelagia, New Sonne, Huna, and Penumbra. Squat lobsters of the genus Munidopsis are also common at the margins of individual fields.

The mussel *Bathymodiolus septemdierum* Hashimoto & Okutani, 1994, limpets of the genus *Lepetodrilus*, and gastropods of the genus *Phymorhynchus* occur at all newly discovered vent fields (Fig. 5B-C). In contrast, the hairy gastropod *Alviniconcha marisindica* Okutani, 2014 and the “scaly-foot” gastropod *Chrysomallon squamiferum*[35] were not observed at all fields (Fig. 5A + D-G), and their distribution is listed in STable 2. At Pelagia, *C. squamiferum* shows a morphotype different from those previously described[35], with a dark shell and white sclerites (Fig. 5E). Other gastropods, including provannid and skeneid snails, slit limpets, and phenacolepadid limpets, are also well represented.

One of the most diverse groups occurring in these areas is Annelida (Fig. 6). Among the free-living polychaetes, the family *Polynoidae* is represented by several taxa, including *Cladopolynoe jiaolongae* (Han, Zhou, Chen & Wang, 2023), *Photinopolynoe kaireiensis* (Han, Zhou, Chen & Wang, 2023), *Stratigos bipapillata* (Zhou, Wang, Zhang & Wang, 2018), *Levensteiniella spp*., and several undescribed species. *Archinome jasoni* Borda, Kudenov, Chevaldonné, Blake, Desbruyères, Fabri, Hourdez, Pleijel, Shank, Wilson, Schulze & Rouse, 2013 and *Hesiolyra heteropoda* Wang, Xu, Zhang, Zhou, Liu, Chen, Watanabe & Qiu, 2020 were also observed. Sedentary polychaetes, mainly belonging to the families Spionidae, Terebellidae, Ampharetidae, including *Amphisamytha marisindica* Zhou, Chen, Sun, Watanabe, Zhang & Wang, 2019 and A. *wocanensis* Zhou, Chen, Sun, Watanabe, Zhang & Wang, 2019, and *Alvinellidae*, including *Paralvinella mira* Han, Zhang, Wang & Zhou, 2021, show variable abundances among the vent fields (Fig. 6A-B; STable 2). The presence of *Branchipolynoe longqiensis* Zhou, Zhang, Lu & Wang, 2017, a polynoid associated with *Bathymodiolus septemdierum*, was observed, with infestation rates ranging from none to up to seven individuals per host.

In the peripheral zones of active vent sites, extensive areas are covered by at least two species of sea anemones, *Maractis spp*. (Fig. 7B–C). Closer to the vents, the substrate is densely populated by larger individuals, whereas with increasing distance from chimney structures, individuals become more sparse and smaller. Other groups, such as the zoarcid fish *Pachycara angeloi* Thiel, Knebelsberger, Kihara & Gerdes, 2021, chiridotid holothurians, aplacophoran molluscs, nemerteans, and platyhelminths, are reported from most vent fields (Fig. 7A, D–E); their distribution is listed in STable 2.

It is important to note that, excluding *Chrysomallon squamiferum*, no other representatives of the family Peltospiridae were observed in the investigated new vent fields. The distribution of *Gigantopelta aegis* Chen, Linse, Roterman, Copley & Rogers, 2015, *Dracogyra subfusca* Chen, Zhou, Wang & Copley, 2017, and *Lirapex politus* Chen, Zhou, Wang & Copley, 2017 appears to be restricted to the SWIR[18, 35, 36]. The same applies to *Kiwa tyleri* Thatje, 2015, which has been reported from the Duanqiao and Longqi vent fields[18, 37, 38].

5.1 Faunal zonation

5.1.1 Active hydrothermal vent fields

The general faunal zonation is similar to that described in the previous literature[39], and the discharge of hydrothermal fluids is considered the driving factor for the spatial distribution and abundance of vent fauna[40–42] (Fig. 8A).

The central zone of active hydrothermal vents is generally populated by dense aggregations of *R. kairei* (Fig. 8B), followed by clusters of *A. marisindica* and *C. squamiferum* with *A. rodriguezensis* (Fig. 8C) and *Phymorhynchus* spp. occurrences (Fig. 8E). In some cases, *P. mira* can also be found in high-temperature discharge zones of individual chimneys (Fig. 6A-B). *Bathymodiolus septemdierum* dominates the transition zone into distal fields of anemones but can occur within these fields as well (Fig. 8D).

At the periphery, *Maractis* spp. is one of the most abundant groups in combination with other taxa, including *Phymorhynchus* spp., *N. marisindica*, *Munidopsis* spp., Chiridotidae holothurians and Zoarcidae fish (Fig. 8E). Single individuals of *R. kairei* were observed in the periphery and this pattern can be related to a migrating behavior of this taxon[39, 43].

5.1.2 Inactive hydrothermal sites

Hydrothermally inactive sites show megafauna assemblages considerably different from active fields both, in terms of species composition and abundance[44]. Depending on the proximity to active vent sites, inactive sites can have different faunal compositions (Fig. 9). Assemblages close to active sites display a mix of non-vent species and a reduced number of vent species in low abundances[45] .When spatially separated from active sites, the assemblages may represent a distinct deep-sea habitat[45, 46].

Although focused on megafauna along the CIR and SEIR, information regarding the microbial community is presented elsewhere[47, 48]. Detailed studies addressing taxonomy and connectivity across different faunal size classes are also available[49–54]. Larval development and bioturbation processes have been examined in previous works[45, 55, 56].

6 Implications

The discovery of thirteen previously unknown hydrothermal vent fields and associated SMS occurrences along the southern CIR and northern SEIR substantially expands the documented extent of hydrothermal activity in the central Indian Ocean. The distribution of the new occurrences across axial valley, ridge-flank, off-axis volcanic-plateau, and non-transform-offset settings shows that hydrothermal circulation in the INDEX area is not restricted to the axial valley. Instead, it is controlled by the combined effects of magmatic heat supply, fault-controlled permeability, crustal age, and local lithological architecture. Seafloor massive sulfide mineralization on ridge flanks, within non-transform offsets, and on an off-axis volcanic plateau up to 17 km from the present spreading axis shows that favourable conditions for hydrothermal circulation can persist or be reactivated beyond the zone of active crustal accretion. Thus, in the INDEX area, the key predictor for hydrothermal circulation is not simply proximity to the spreading axis, but the combination of residual or renewed heat supply with fault-controlled permeability.

The massive sulfide occurrences in the INDEX area display a range of mineralization styles, including active Cu-rich black smoker chimneys, sulfide mounds with Zn- and silica-bearing peripheral facies, silica-rich hydrothermal deposits, oxidized inactive mounds, and dispersed mound fields developed in fault-controlled settings. However, the mineralogical and geochemical data do not define fundamentally new mineralization types. Instead, they show that the compositional range typical of MOR-related SMS mineralization is developed across several structural and lithological environments along the southern CIR and northern SEIR. A central metallogenic implication is that the most favourable settings in the INDEX area are not restricted to the axial valley or to obvious mafic–ultramafic exposures. The off-axis volcanic plateau fields Huna, Penumbra, Lux, and Umbra show that basalt-hosted SMS occurrences can form and be preserved where ridge-parallel fault systems, local volcanic or thermal anomalies, and prolonged hydrothermal circulation coincide. This is particularly relevant for Lux, where hydrothermal activity is expressed by numerous small and dispersed mounds rather than by a single large active chimney complex. Such field relationships indicate that inactive or weakly venting SMS occurrences may be underrepresented if exploration relies mainly on strong plume signals or visually obvious black smoker systems. Mafic- to ultramafic-influenced systems, including Kaimana, Sooraj, and Jim, add an additional lithological and structural component to the INDEX dataset. Their significance lies primarily in the exposure or involvement of deeper oceanic crust and upper mantle lithologies within structurally complex settings, rather than in the definition of a distinct geochemical mineralization type based on surface samples. Thus, the metallogenic significance of the INDEX area lies in the coexistence of several favourable factors: structurally focused fluid pathways, basaltic to mafic–ultramafic host rocks, phase separation, and repeated or prolonged hydrothermal activity across axial and off-axis settings.

The INDEX occurrences also capture a broad temporal spectrum of hydrothermal system evolution. This spectrum ranges from relatively young active chimney growth at Alpha, through mature and probably longer-lived high-temperature chimney complexes such as Kairei and Edmond, to systems recording changes in hydrothermal conditions, as observed at Huna, where sulfide-rich mineralization was overprinted by silica-rich precipitation, probably in response to changing fluid temperature and chemistry. Surya appears to represent a waning system, with preserved evidence for earlier high-temperature mineralization but only low-temperature diffuse discharge of about 31°C at present. Further along this evolutionary sequence, Gauss and Score represent recently inactive systems with well-preserved chimney structures, whereas Lux, Umbra and the southern part of Jim likely represent older inactive systems, where mound morphologies have been strongly modified by oxidation, mass wasting, erosion, and flattening. Together, these relationships show that the INDEX area preserves not only diverse tectonic and lithological settings, but also different stages in the life cycle of SMS-forming hydrothermal systems.

This combination of structural, lithological, and temporal variability is consistent with regional geodynamic models that describe the Rodrigues Triple Junction as a structurally complex and dynamically evolving ridge system, rather than a simple steady-state spreading-center environment[57]. It also fits broader models in which magma supply provides a first-order control on hydrothermal activity, but permeability, tectonic segmentation, and additional or prolonged heat sources can strongly influence where hydrothermal systems and SMS accumulations develop[58]. From a resource-assessment perspective, the present data do not quantify recoverable resources or subsurface continuity. They do, however, broaden the range of geological settings that should be considered in future assessments of SMS occurrences in the central Indian Ocean.

The hydrothermal communities observed at the newly discovered SMS occurrences support the interpretation of the Indian Ocean as a distinct but interconnected hydrothermal biogeographic province. Dominant taxa such as *Rimicaris kairei* and *Chrysomallon squamiferum* link the new fields with known CIR and SWIR vent fauna. At the same time, local differences in species occurrence, including the unusual *C. squamiferum* morphotype observed at Pelagia, highlight the need for further taxonomic, population-genetic, and connectivity studies. Because the new fields include both active vent communities and inactive SMS habitats, they provide a comparative basis for assessing how vent activity, substrate type, and site isolation influence biodiversity patterns across the CIR–SEIR system.

The presented results demonstrate the value of an integrated exploration strategy for identifying both active vent fields and inactive SMS occurrences. Water-column plume detection remains essential for locating active discharge, but it is insufficient on its own for recognizing inactive, weakly venting, diffuse, or particle-poor systems. In the INDEX area, the combination of regional bathymetry, plume surveys, near-bottom high-resolution mapping, self-potential measurements, and targeted ROV ground-truthing enabled the recognition of a broader range of hydrothermal expressions, including active black smokers,

diffuse discharge sites, oxidized mounds, silica-rich deposits, and fault-controlled inactive occurrences. Future exploration strategies in comparable ridge systems should therefore include off-axis volcanic plateaus, ridge-parallel fault zones, tectonic grabens, and non-transform discontinuities, rather than focusing only on axial black-smoker systems.

7 Conclusion

This study presents the first integrated documentation of thirteen newly discovered hydrothermal vent fields and associated SMS occurrences along the southern Central Indian Ridge and northern Southeast Indian Ridge, including the first confirmed vent fields on the SEIR. Together with the previously known Kairei and Edmond systems, these discoveries establish the region around the Rodrigues Triple Junction as one of the most densely documented areas of hydrothermal activity and SMS formation in the Indian Ocean. The new vent fields are distributed across axial valley, ridge-flank, off-axis volcanic-plateau, and non-transform-offset settings, demonstrating that hydrothermal circulation in the INDEX area is controlled by the interplay of magmatic heat supply, fault-controlled permeability, crustal age, and local lithological architecture. Mineralogical and geochemical data show that the occurrences are broadly consistent with MOR-related SMS systems, while also documenting variability in mineralization style, preservation state, fluid composition, host-rock association, and stage of hydrothermal evolution. By integrating geological observations, seafloor imagery, mineralogical and geochemical data, hydrothermal fluid chemistry, and megafaunal observations, this study provides a baseline characterization of the newly discovered fields. The dataset forms a reference for future work on subsurface architecture, resource assessment, biodiversity, habitat distribution, environmental monitoring, and the evolution of hydrothermal systems along the Central and Southeast Indian Ridges.

8 Methodology

8.1 Geological mapping, sampling, and analyses

For regional reconnaissance and early-stage prospecting, comprehensive bathymetric surveys were carried out along the southern CIR and northern SEIR segments during two cruises using vessel-mounted swath echosounder systems, mainly Simrad Kongsberg EM 120 and EM 122. The resulting bathymetric maps, with a resolution of approximately 40 m, were used to plan tow-yo tracks through prospective areas for near-bottom plume reconnaissance using a dedicated sensor sled. The tow-yo tracks ranged from 40 to 400 m above the seafloor, while the vessel followed pre-planned tracks at about 1.5 kn. The sensor sled was equipped with a standard conductivity–temperature–depth (CTD) system coupled with auxiliary sensors for optical light scattering and redox potential.

Once a hydrothermal anomaly was detected in the near-bottom water column, the respective area was mapped with the custom-built deep-towed bathymetry sled HOMESIDE. HOMESIDE was equipped with an EM2040 swath echosounder and a self-potential sensor system and was towed at speeds of up to 2.5 kn, approximately 100 m above the seafloor. This setup produced bathymetric maps with swath widths of approximately 700 m and a spatial resolution of about 2 m. In addition, near-bottom water-column data were collected to detect buoyant plume signals above active hydrothermal vents. Inactive hydrothermal mounds were recognized from their characteristic size and morphology in digital elevation models and, in some cases, by distinct self-potential anomalies and characteristic surface features in backscatter data.

After localization of a vent field, remotely operated vehicles, in most cases the Canadian ROV ROPOS operated by the Canadian Scientific Submersible Facility, were used for ground-truthing, sampling, and optical geological mapping using video, photography, and photogrammetry. For sampling, the ROVs were equipped with manipulators, push cores, suction samplers, hydrothermal fluid samplers such as the custom-built Kiel Pumping System (KIPS), and BGR's Remotely-operated Coring System (ROCS) drilling tool, which is capable of drilling up to four 1 m cores from outcropping massive sulfides or host rocks per dive.

Whole-rock analyses of polymetallic sulfides were conducted at Activation Laboratories Ltd. in Ancaster, Canada. Bulk concentrations of major, minor, trace, and ultra-trace elements, as well as sulfur, were determined using a combination of analytical techniques, including ICP-MS, ICP-OES, neutron activation analysis, and infrared spectroscopy. Repeated analyses of reference materials, duplicates, and analytical blanks were performed for quality control. The mineralogy of massive sulfides and associated altered host-rock lithologies was studied on representative polished thin and thick sections using optical microscopy, and scanning electron microscopy (SEM).

Hydrothermal fluids were collected using the BGR-KIPS flow-through sampling system mounted on the ROV. The inert PFA/PTFE–titanium system allows contamination-free sampling of high-temperature fluids and is guided in situ by a real-time temperature probe for precise positioning at vent orifices. After recovery, all KIPS flasks were processed immediately following a standardized protocol. High-temperature fluids were left unfiltered, whereas diffuse fluids were filtered through 0.2 µm filters to remove suspended particles. Subsamples were taken for pH, Eh, conductivity/salinity, dissolved H_2S, and major- and trace-element analyses. Endmember quality was assessed using Mg and Cl concentrations, with most focused-flow samples containing > 90% hydrothermal fluid. Ex situ pH, Eh, and salinity were measured on board, while major and trace elements, including metals and REE, were later analyzed by ICP-OES and ICP-MS at Kiel University after matrix separation.

8.2 Biological imaging acquisition and annotation

Eight expeditions conducted between 2013 and 2019 and between 2021 and 2023, comprising a total of 153 stations, were used for the imaging studies. Together, these surveys covered a cumulative bottom-track distance of 606,612 m and yielded 94,123 photographs, 94,508 frame grabs, and 1,015 hours of video imagery. All photographs were reviewed, and faunal occurrences were annotated and extracted. The term annotation is defined as the assignment of a semantic category (morphotype), a label that is positioned in a region of interest within a photograph or video. Video imagery was used only when additional images were required to clarify imagery-based identifications. The study area spans a bathymetric range from 1,581 to 3,710 m. All imaging transects were

conducted using three different video sleds and remotely operated vehicles. The number of stations and images collected at each locality, as well as the technical specifications of the gear used, are provided in STables 7A–B.

Annotation and taxonomic identification were carried out as described in previous literature[59]. All annotated taxa are listed for each field within active and inactive SMS occurrences, as well as within the host-rock periphery and non-vent areas (STables 2–6). The host-rock periphery is defined as non-vent substrate, such as MOR basalt and pelagic sediment, extending from the immediate vicinity of hydrothermal occurrences to a distance of 500 m. All taxa identified at distances of 500 m or more from hydrothermal occurrences are considered non-vent taxa. In total, 28,916 annotations identified 305 taxonomic morphotypes across all stations. Within active vent fields, 163 taxa were identified, of which 20 were associated only with active and diffuse venting areas (STables 2 and 3). In inactive fields, 129 taxa were identified, including six taxa found exclusively at inactive sites (STable 4). In the periphery of active vent fields and inactive sites, 199 taxa were identified, including 14 taxa restricted to the host-rock periphery (STable 5). Non-vent areas hosted 237 taxa, of which 57 occurred only in non-vent areas (STable 6).

Declarations

Competing interests

The authors declare no competing interests.

Funding

The investigations presented in this study were funded by the Federal Institute for Geosciences and Natural Resources (BGR), Hannover, Germany, within the framework of its exploration contract with the International Seabed Authority.

Author Contribution

This manuscript is based on data acquired within the framework of BGR's long-term INDEX exploration program. S.F. and T.Ku. developed the concept of the manuscript and coordinated the integration of the geological, geochemical, fluid-chemical, and biological datasets. Geological and volcanological data used in this study were compiled and interpreted by T.Ku., S.F., U.S.S., R.F., and M.K. Mineralogical and bulk-geochemical data were compiled and interpreted by S.F. and U.S.S. Hydrothermal fluid data were provided and interpreted by D.G.-S. Biological imagery data, faunal annotations, and biological interpretations were contributed by T.Ki. and K.M. S.F. prepared the initial manuscript draft with contributions from T.Ku., T.Ki., K.M., U.S.S., and D.G.-S. All authors contributed to manuscript review and editing and approved the final version.

Acknowledgement

This work is the result of more than a decade of prospecting and exploration for polymetallic massive sulfides and associated hydrothermal vent systems along the southern Central Indian Ridge and northern Southeast Indian Ridge within BGR's ISA exploration contract area. We thank all colleagues working within the INDEX project who contributed to expedition planning, field operations, sampling, sample processing, data analysis, and interpretation across multiple cruises. In particular, we acknowledge Hendrik Müller, Stephanie Bellenberg, Udo Barckhausen, Katrin Schwalenberg, Ingo Heyde, Stephan Deike, Kornelia Dietzel, Simone Sturm, Henning Wedemeyer, Harold Gibson, Thomas Gemmel, Sven Petersen, Sebastian Graber, Katharina Kniesz, Cornelia Kriete, Ulrike Westernströer, Karen Bremer, and Heiko Jähmlich for their contributions. We are deeply indebted to the captains, officers, and crews of the participating research vessels, especially FS SONNE, FS Maria S. Merian, and RV Pelagia, for their outstanding support under demanding offshore conditions. We further acknowledge the ROV teams of Jason, Kiel 6000, and particularly ROV ROPOS of the Canadian Scientific Submersible Facility, whose operations were essential for seafloor imaging, ground-truthing, and safe sampling at active and inactive vent sites and their surroundings.The investigations presented here were funded by the Federal Institute for Geosciences and Natural Resources (BGR), Hannover, Germany, within the framework of its exploration contract with the International Seabed Authority.

Data Availability

All data generated or analysed within the scope of this study are included in this submission. The Supplementary Information contains detailed additional datasets, figure plates and tables supporting the interpretations presented in the main text. References to Supplementary Information within the manuscript are indicated as SFigures and STables.

References

1. Corliss, J. B. & Ballard, R. D. Submarine thermal springs on the Galápagos Rift. *Science* **203**, 1073–1083. https://doi.org/10.1126/science.203.4385.1073 (1979).
2. Beaulieu, S. E. & Szafrański, K. M. InterRidge Global Database of Active Submarine Hydrothermal Vent Fields Version 3.4. (2020). https://doi.org/10.1594/PANGAEA.917894

3. Wang, Y. et al. Mineralogy and trace element geochemistry of sulfide minerals from the Wocan Hydrothermal Field on the slow-spreading Carlsberg Ridge, Indian Ocean. *Ore Geol. Rev.* **84**, 1–19. https://doi.org/10.1016/j.oregeorev.2016.12.020 (2017).
4. Qiu, Z. et al. The temporal variability of hydrothermal activity of Wocan hydrothermal field, Carlsberg Ridge, northwest Indian Ocean. *Ore Geol. Rev.* **132**, 103999. https://doi.org/https://doi.org/10.1016/j.oregeorev.2021.103999 (2021).
5. Wang, Y. et al. The Daxi Vent Field: An active mafic-hosted hydrothermal system at a non-transform offset on the slow-spreading Carlsberg Ridge, 6°48'N. *Ore Geol. Rev.* **129**, 103888. https://doi.org/https://doi.org/10.1016/j.oregeorev.2020.103888 (2021).
6. Qiu, Z. et al. Discovery of the Tianxiu hydrothermal field on the Carlsberg Ridge, Indian Ocean. *Front. Earth Sci.* **9**, 728392. https://doi.org/10.3389/feart.2021.728392 (2021).
7. Qiu, Z. et al. Discovery and characterization of a new hydrothermal field (Tianshi) at 2° N on the slow-spreading Carlsberg Ridge. *Acta Oceanol. Sin*. **43**, 545–559. https://doi.org/10.1007/s13131-024-2369-5 (2024).
8. Kim, J. et al. Discovery of active hydrothermal vent fields along the Central Indian Ridge (8–12°S). *Geochem. Geophy. Geosy*, 21, e2020GC009058 (2020). https://doi.org/10.1029/2020GC009058
9. Nakamura, K. et al. Discovery of new hydrothermal activity and chemosynthetic fauna on the Central Indian Ridge at 18°–20°S. *Plos One*. **7**, e32965. https://doi.org/10.1371/journal.pone.0032965 (2012).
10. Tamaki, K. & Shipboard, S. Dodo and Solitaire hydrothermal fields: new discoveries at the Central Indian Ridge. *AGU Fall Meeting Abstracts* (2010). https://ui.adsabs.harvard.edu/abs/2010AGUFMOS21A1468T/abstract
11. Van Dover, C. L. et al. Biogeography and Ecological Setting of Indian Ocean Hydrothermal Vents. *Science* **294**, 818. https://doi.org/10.1126/science.1064574 (2001).
12. Hashimoto, J. First hydrothermal vent communities from the Indian Ocean discovered. *Zoo Stud.* **18**, 717–721. https://doi.org/10.2108/zsj.18.717 (2001).
13. Gamo, T. et al. Chemical characteristics of newly discovered black smoker fluids and associated hydrothermal plumes at the Rodriguez Triple Junction, Central Indian Ridge. *Earth Planet. Sc Lett.* **193**, 371–379. https://doi.org/https://doi.org/10.1016/S0012-821X(01)00511-8 (2001).
14. Herzig, P. M. & Plueger, W. L. Exploration for hydrothermal activity near the Rodriguez triple junction, Indian Ocean. *Can. Mineral.* **26**, 721–736 (1988).
15. Plüger, W. et al. Discovery of hydrothermal fields at the Central Indian Ridge. *Mar. Min.* **9**, 255–269 (1990).
16. Tao, C. et al. Seafloor hydrothermal activity and polymetallic sulfide exploration on the Southwest Indian Ridge. *Chin. Sci. Bull.* **59**, 2266–2276. https://doi.org/10.1007/s11434-014-0182-0 (2014).
17. Copley, J. T. et al. Ecology and biogeography of megafauna and macrofauna from the first known hydrothermal–vent field on the very slow spreading Southwest Indian Ridge. *Sci. Rep.* **6**, 39158. https://doi.org/10.1038/srep39158 (2016).
18. Zhou, Y. et al. Characterization of vent fauna at three hydrothermal vent fields on the Southwest Indian Ridge: Implications for biogeography and interannual dynamics on ultraslow-spreading ridges. *Deep-Sea Res. I: Oceanogr. Res. Pap*. **137**, 1–12. https://doi.org/https://doi.org/10.1016/j.dsr.2018.05.001 (2018).
19. Watanabe, H. K. et al. Phylogeography of hydrothermal vent stalked barnacles: a new species fills a gap in the Indian Ocean 'dispersal corridor' hypothesis. *Roy Soc. Open. Sci.* **5**, 172408. https://doi.org/10.1098/rsos.172408 (2018).
20. Carbotte, S. M., Smith, D. K., Cannat, M. & Klein, E. M. Tectonic and magmatic segmentation of the Global Ocean Ridge System: a synthesis of observations In Magmatic Rifting and Active Volcanism. Vol. 420 (eds Wright, T. J. et al.) 249–295 (Geological Society Special, (2016).
21. Bartsch, C. *Structural and magnetic investigations of two spreading segments of the Southwest Indian Ridge.* Dissertation thesis, Universität Bremen, (2014).
22. Jamieson, J. W. & Gartman, A. Defining active, inactive, and extinct seafloor massive sulfide deposits. *Mar. Policy*. **117** https://doi.org/10.1016/j.marpol.2020.103926 (2020).
23. Franklin, J. M., Gibson, H. L., Jonasson, I. R. & Galley, A. G. Volcanogenic massive sulfide deposits In Economic Geology 100th Anniversary Volume. (eds Hedenquist, J. W., Thompson, J. F. H., Goldfarb, R. J. & Richards, J. P.) (Society of Economic Geologists, (2005).
24. Gibson, H. L. Volcano-hosted ore deposits In Volcanoes and the Environment. (eds Ernst, G. G. J., Marti & Joan) 333–386 (Cambridge University Press, (2005).
25. German, C. R. & Von Damm, K. L. 6.07 - Hydrothermal Processes In Treatise on Geochemistry. (eds Holland, H. D. & Turekian) (2003)., K. K.) 181–222 (Elsevier/Pergamon.
26. Seyfried, W. E., Pester, N. J., Tutolo, B. M. & Ding, K. The Lost City hydrothermal system: Constraints imposed by vent fluid chemistry and reaction path models. *Geochim. Cosmochim. Ac*. **75**, 1574–1593. https://doi.org/10.1016/j.gca.2010.12.013 (2011).
27. Butterfield, D. A., Massoth, G. J., McDuff, R. E., Lupton, J. E. & Lilley, M. D. Geochemistry of hydrothermal fluids from the northern Juan de Fuca Ridge: Fluid–mineral equilibrium and stable isotope constraints. *J. Geophys. Res.* **102**, 12245–12266. https://doi.org/10.1029/96JB03804 (1997).
28. Von Damm, K. L. Controls on the chemistry and temporal variability of seafloor hydrothermal fluids In *Seafloor Hydrothermal Systems: Physical, Chemical, Biological, and Geological Interactions.* Vol. 91 (eds. Humphris, S. E., Zierenberg, R. A., Mullineaux, L. S., & Thomson, R. E.) 222–247 (American Geophysical Union, 1995).
29. Douville, E. et al. The fate of metals in hydrothermal fluids: Venting at the Mid-Atlantic Ridge. *Chem. Geol.* **184**, 37–48. https://doi.org/10.1016/S0009-2541(01)00351-3 (2002).
30. Gallant, R. M. & Von Damm, K. L. Geochemical controls on hydrothermal fluids from the Kairei and Edmond Vent Fields, 23°-25°S, Central Indian Ridge. *Geochem. Geophy Geosy*. **7**, 1–24. https://doi.org/10.1029/2005GC001067 (2006).

31. Fontaine, F. J. & Wilcock, W. S. D. Dynamics and heat transfer of high-temperature hydrothermal plumes over spreading centers. *Geochem. Geophy Geosy*. **7** https://doi.org/10.1029/2005GC001234 (2006).
32. Mosier, D. L., Singer, D. A. & Berger, V. I. Volcanogenic Massive Sulfide Deposit Density. Report No. U.S. Geological Survey Scientific Investigations Report 2007–5082, 21 (2007). https://doi.org/https://doi.org/10.3133/sir20075082
33. Hannington, M., Jamieson, J., Monecke, T. & Petersen, S. Modern sea-floor massive sulfides and base metal resources: toward an estimate of global sea-floor massive sulfide potential. *Rev. Econ. Geol. Spec. Pub*. **15**, 317–337 (2010).
34. Hannington, M. D., de Ronde, C. D. J. & Petersen, S. Sea-floor tectonics and submarine hydrothermal systems In *Economic Geology 100th Anniversary Volume.* (eds. Hedenquist, J. W., Thompson, J. F. H., Goldfarb, R. J., & Richards, J. P.) 111–141 (Society of Economic Geologists, 2005).
35. Chen, C., Copley, J. T., Linse, K. & Rogers, A. D. Low connectivity between 'scaly-foot gastropod' (Mollusca: Peltospiridae) populations at hydrothermal vents on the Southwest Indian Ridge and the Central Indian Ridge. *Org. Divers. Evol.* **15**, 663–670. https://doi.org/10.1007/s13127-015-0224-8 (2015).
36. Chen, C., Zhou, Y., Wang, C. & Copley, J. T. Two New Hot-Vent Peltospirid Snails (Gastropoda: Neomphalina) from Longqi Hydrothermal Field, Southwest Indian Ridge. *Front. Mar. Sci.* **4** https://doi.org/10.3389/fmars.2017.00392 (2017).
37. Copley, J. T. et al. Ecology and biogeography of megafauna and macrofauna at the first known deep-sea hydrothermal vents on the ultraslow-spreading Southwest Indian Ridge. *Sci. Rep.* **6** https://doi.org/10.1038/srep39158 (2016).
38. Zhang, D., Zhou, Y., Cheng, H. & Wang, C. The complete mitochondrial genome of a yeti crab Kiwa tyleri Thatje, 2015 (Crustacea: Decapod: Anomura: Kiwaidae) from deep-sea hydrothermal vent. *Mitocondr DNA B*. **2**, 141–142. https://doi.org/10.1080/23802359.2017.1289347 (2017).
39. Watanabe, H. & Beedessee, G. Vent Fauna on the Central Indian Ridge In Subseafloor Biosphere Linked to Hydrothermal Systems. (eds Ishibashi, J., Okino, K. & Sunamura, M.) 205–212 (Springer Japan, (2014).
40. Copley, J. T. P., Jorgensen, P. B. K. & Sohn, R. A. Assessment of decadal-scale ecological change at a deep Mid-Atlantic hydrothermal vent and reproductive time-series in the shrimp Rimicaris exoculata. *J. Mar. Biol. Assoc. Uk*. **87**, 859–867. https://doi.org/10.1017/s0025315407056512 (2007).
41. Juniper, S. K., Jonasson, I. R., Tunnicliffe, V. & Southward, A. J. Influence of a tube-building polychaete on hydrothermal chimney mineralization. *Geology* **20**, 895. https://doi.org/10.1130/0091-7613(1992)020 (1992).
42. Sen, A. et al. Community succession in hydrothermal vent habitats of the Eastern Lau Spreading Center and Valu Fa Ridge, Tonga. *Limnol. Oceangr*. **59**, 1510–1528. https://doi.org/10.4319/lo.2014.59.5.1510 (2014).
43. Beedessee, G. et al. High Connectivity of Animal Populations in Deep-Sea Hydrothermal Vent Fields in the Central Indian Ridge Relevant to Its Geological Setting. *Plos One*. **8**, e81570. https://doi.org/10.1371/journal.pone.0081570 (2013).
44. Boschen, R. E., Rowden, A. A., Clark, M. R., Pallentin, A. & Gardner, J. P. A. Seafloor massive sulfide deposits support unique megafaunal assemblages: Implications for seabed mining and conservation. *Mar. Environ. Res.* **115**, 78–88. https://doi.org/10.1016/j.marenvres.2016.02.005 (2016).
45. Gerdes, K., Martínez Arbizu, P., Schwarz-Schampera, U., Schwentner, M. & Kihara, T. C. Detailed Mapping of Hydrothermal Vent Fauna: A 3D Reconstruction Approach Based on Video Imagery. *Front Mar. Sci* **6** (2019).
46. Van Dover, C. L. Inactive Sulfide Ecosystems in the Deep Sea: A Review. *Front. Mar. Sci.* **6** https://doi.org/10.3389/fmars.2019.00461 (2019).
47. Adam, N. et al. Microbial Community Compositions and Geochemistry of Sediments with Increasing Distance to the Hydrothermal Vent Outlet in the Kairei Field. *Geomicrobiol. J.* **37**, 242–254. https://doi.org/10.1080/01490451.2019.1694107 (2019).
48. Adam-Beyer, N. et al. Microbial ecosystem assessment and hydrogen oxidation potential of newly discovered vent systems from the Central and South-East Indian Ridge. *Front. Microbiol.* **14**, 1173613 (2023).
49. Hoffman, L., Kniesz, K., Martínez Arbizu, P. & Kihara, T. C. Abyssal vent field habitats along plate margins in the Central Indian Ocean yield new species in the genus Anatoma (Vetigastropoda: Anatomidae). *Eur. J. Taxonomy*. **826**, 135–162. https://doi.org/10.5852/ejt.2022.826.1841 (2022).
50. Thiel, R., Knebelsberger, T., Kihara, T. & Gerdes, K. Description of a new eelpout Pachycara angeloi sp. nov. (Perciformes: Zoarcidae) from deep-sea hydrothermal vent fields in the Indian Ocean. *Zootaxa* **4980** https://doi.org/10.11646/zootaxa.4980.1.6 (2021).
51. Kniesz, K., Jażdżewska, A. M., Martínez Arbizu, P. & Kihara, T. C. DNA Barcoding of Scavenging Amphipod Communities at Active and Inactive Hydrothermal Vents in the Indian Ocean. *Front. Mar. Sci.* **8** https://doi.org/10.3389/fmars.2021.752360 (2022).
52. Kniesz, K., Hoffman, L., Martínez Arbizu, P. & Kihara, T. C. High genomic connectivity within Anatoma at hydrothermal vents along the Central and Southeast Indian Ridge. *Sci. Rep.* 15, (1971). (2025) https://doi.org/10.1038/s41598-025-85507-z
53. Neufeld, M., Meyn, K., Kihara, T. C., Martinez Arbizu, P. & Kuhn, T. First record of the giant anemone, Relicanthus daphneae, at active hydrothermal vent fields in the Indian Ocean. *J. Mar. Biol. Assoc. Uk*. **104** https://doi.org/10.1017/s0025315424001127 (2024).
54. Wieschermann, L. & Kihara, T. C. A new species of the genus Aphotopontius Humes, 1987 (Siphonostomatoida, Dirivultidae) from a vent field at the Southeast Indian Ridge. *Plank Benthos Res.* **20**, s102–s120. https://doi.org/10.3800/pbr.20.s102 (2025).
55. Demidow, O., Kihara, T. C., Arbizu, P. M. & Clark, P. F. The megalopal stage of the hydrothermal vent crab Austinograea rodriguezensis Tsuchida amp; Hashimoto, 2002 (Decapoda: Bythograeidae): a morphological description based on CLSM images. *Zootaxa* **5040**, 365–387. https://doi.org/10.11646/zootaxa.5040.3.3 (2021).
56. Kihara, T. C., Clark, P. F. & Meyn, K. H. First zoeal stage of the Indian Ocean hydrothermal vent crab, Austinograea rodriguezensis Tsuchida & Hashimoto, 2002 (Decapoda: Brachyura: Bythograeidae). *Zootaxa* **5476**, 192–206. https://doi.org/10.11646/zootaxa.5476.1.18 (2024).
57. Meyzen, C. M. & Schwarz-Schampera, U. The complex Rodrigues triple junction migration since ca. 8 Ma: A response to episodic Amsterdam–St. *Paul hotspot tail capture Southeast. Indian Ridge? Geology*. **51**, 823–828. https://doi.org/10.1130/G51131.1 (2023).
58. Baker, E. T. & German, C. R. On the Global Distribution of Hydrothermal Vent Fields. *Geophys. Monogr. Ser.* **148**, 245–266. https://doi.org/10.1029/148GM10 (2004).

59. Gerdes, K. et al. Megafauna of the German exploration licence area for seafloor massive sulphides along the Central and South East Indian Ridge (Indian Ocean). *Biodivers. Data J.* **9**, e69955 (2021).

Tables

Table 1: Overview of the discovered SMS occurrences within the BGR study area, including the previously known Edmond and Kairei fields. The table summarizes discovery year, discovery method, years of investigation, tectonic setting, host rock, water depth, location, surface area, number of sites, and activity status.

Cluster	Field	Year of discovery	Discovered with	Year studied	Tectonic Setting	Host rock	Depth (m.b.s.l)	Latitude	Longitude	Surface area (m^2)	Number of sites
#04	ALPHA	**2015**	indicated buring bathymetric mapping with HMS; confirmed and sampled with ROV ROPOS on R/V Pelagia	2015	non-transform offset	basalt-hosted (D-MORB)	3050	-23.782	69.546	21532	14
#04	EDMOND	**2001**	indicated water column anomaly during survey in 1980s, discovered & confirmed in 2001 with ROV Jason on R/V Knorr	2012, 2013, 2015, 2019	ridge flank	basalt-hosted (D-MORB)	3290	-23.878	69.597	18395	1
#04	GAUSS	**2012**	discovered during video mapping with VS; sampled with TVG on RV Gauss	2012, 2013, 2015, 2019	ridge flank	basalt-hosted (D-MORB)	3050	-23.867	69.607	46785	3
#04	SCORE	**2013**	discovered buring bathymetric mapping with HMS; confirmed and sampled with ROV Kiel 6000 on RV Sonne	2013, 2015, 2019	ridge flank	basalt-hosted (D-MORB)	3200	-23.879	69.608	21834	3
#05	KAIMANA	**2018**	indicated buring bathymetric mapping with HMS; confirmed and sampled with ROV ROPOS on RV Pelagia	2018, 2019	ridge flank	gabbro, troctolite, harzburgite	2675	-25.470	69.931	198787	12
#05	KAIREI	**2000**	plume detected with CTD casts on R/V Hakuho-Maru in 1993; discovery of the active KAIREI mound with ROV Kaiko on R/V Kairei in 2000	2011, 2012, 2013, 2016, 2018, 2019	ridge flank	basalt-hosted (T-MORB, troctolites)	2450	-25.320	70.040	14169	2
#06	SURYA	**2019**	indicated buring bathymetric mapping with HMS; confirmed and sampled with ROV ROPOS on RV Sonne	2019	ridge flank	basalt-hosted (D-MORB)	2925	-25.826	70.125	1954	1

#07	SOORAJ	**2019**	indicated during bathymetric mapping with HMS; confirmed and sampled with ROV ROPOS on RV RELAGIA in 2021	2021, 2022	non-transform offset	ultramafic rock-hosted (gabbro, pyroxenite)	2673	-26.092	70.889	11270	3
#08	PELAGIA	**2014**	detected water column anomaly with PS; confirmed and sampled with ROV ROPOS on RV Pelagia in 2018	2016	axial valley	basalt-hosted (D-MORB)	3660	-26.157	71.437	3175	1
#09	JIM	**2022**	indicated by self potential anomaly with HMS; confirmed and sampled with GC and ROV ROPOS on RV Pelagia	2022	non-transform offset	ultramafic rock-hosted (gabbro, pyroxenite, harzburghite)	2815	-26.464	71.691	84839	15
#11	NEW SONNE	**2017**	indicated by water column anomaly with PS; confirmed and sampled with ROV ROPOS on RV Pelagia in 2018	2017, 2018	axial valley	basalt-hosted (T-MORB)	2930	-27.258	72.724	29861	7
#12	HUNA	**2018**	indicated by self potential anomaly with HMS; confirmed and sampled with ROV ROPOS on RV Sonne in 2019	2018, 2019	off-axis volcanic plateau	basalt-hosted (E-MORB)	2550	-27.639	73.860	32287	14
#12	PENUMBRA	**2018**	indicated by water column anomalywith PS; confirmed and sampled with ROV ROPOS on RV Pelagia in 2018	2018, 2019	off-axis volcanic plateau	basalt-hosted (E-MORB)	2375	-27.635	73.876	48533	16
#12	LUX	**2022**	indicated by shape with HMS; confirmed and sampled with ROV ROPOS on RV Sonne	2022, 2023	off-axis volcanic plateau	basalt-hosted (E-MORB)	2434	-27.629	73.883	8 343 990	> 20
#12	UMBRA	**2022**	detected by gravity	2022	off-axis volcanic	basalt-hosted (E-	2488	-27.617	73.905	631	1

	corer; confirmed with VS in 2023 on RV SONNE	plateau	MORB)

Abbreviations: # = active vent fields that include inactive sites; D-MORB = depleted mid-ocean ridge basalt (La/Sm < 0.8); T-MORB = transitional mid-ocean ridge basalt (La/Sm = 0.8–1.5); E-MORB = enriched mid-ocean ridge basalt (La/Sm > 1.5); PS = plume sled; VS = video sled; HMS = HOMESIDE multibeam bathymetric sled; TVG = TV grab.

Etymology of the discovered vent-field names: Alpha = Greek for “first” or “beginning”, by extension “origin” or “source”; Gauss = named after the research vessel Gauss; Score = Seafloor Confirmed Ore; Kaimana = Hawaiian, derived from *kai* (“sea” or “ocean”) and *mana* (“power”, “force”, or “spiritual energy”), commonly interpreted as “power of the sea” or “ocean energy”; Surya = Sanskrit for “Sun” and also the name of the research vessel used; Sooraj = Hindi for “Sun”, derived from Sanskrit Surya, and also the name of the research vessel used; Pelagia = named after the Dutch research vessel Pelagia; Jim = Just Inactive Mounds; Huna = Hawaiian for “hidden” or “concealed”; Penumbra = Latin for “half-shadow”, referring to the transitional region between light and darkness; Lux = Latin for “light”, also associated with “illumination” and “knowledge”; Umbra = Latin for “shadow”.

Figures

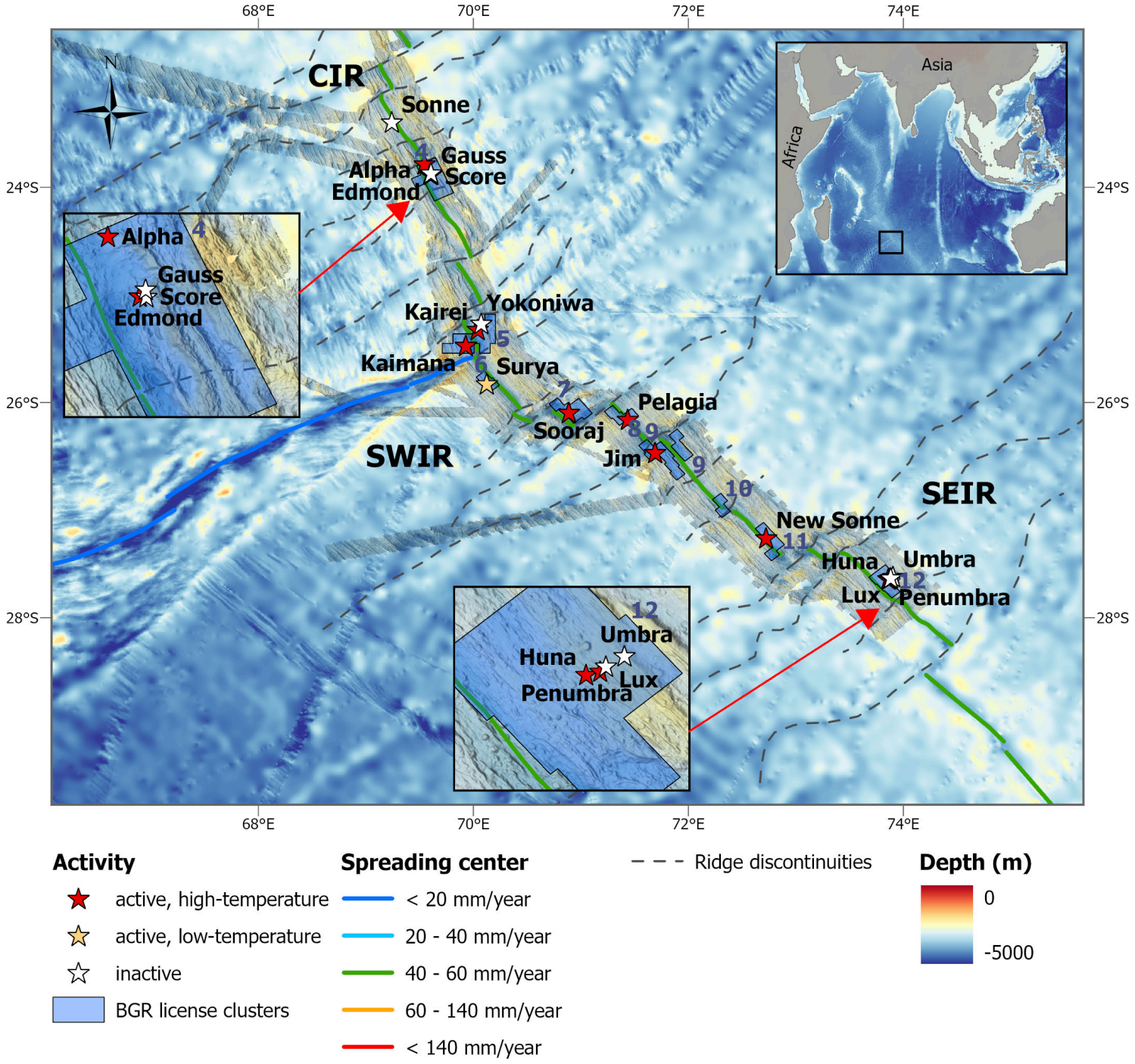


Figure 1

Location of the BGR contract area for the exploration of seafloor massive sulfides (SMS) in the central Indian Ocean around the Rodrigues Triple Junction. The inset shows the regional position of the contract area. The main map shows the 10 × 10 km contract blocks, which are distributed in nine clusters along the southern Central Indian Ridge (CIR) and the northern Southeast Indian Ridge (SEIR) over a total distance of almost 1,000 km. Fifteen hydrothermal vent fields are known within the BGR contract area to date, including the previously known Kaireiand Edmond fields. The Sonne and Yokoniwa vent fields are located outside the BGR contract area. Abbreviation: SWIR = Southwest Indian Ridge.

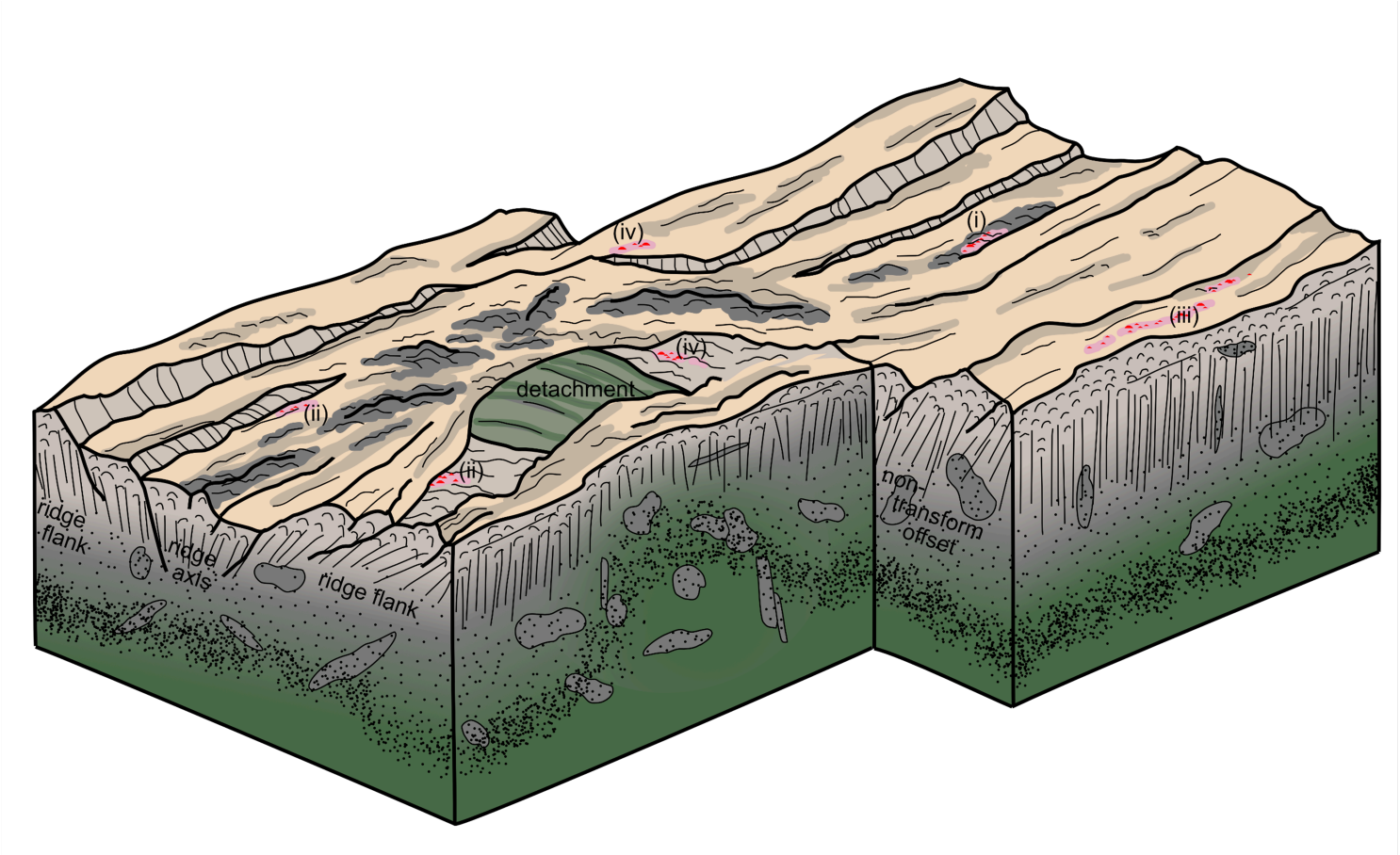


Figure 2

Schematic cross-section through a mid-ocean ridge illustrating the geological and tectonic context of the discovered SMS occurrences. The occurrences are divided into four groups: (i) axial valley group, (ii) ridge-flank group, (iii) off-axis volcanic-plateau group, and (iv) non-transform-offset group.

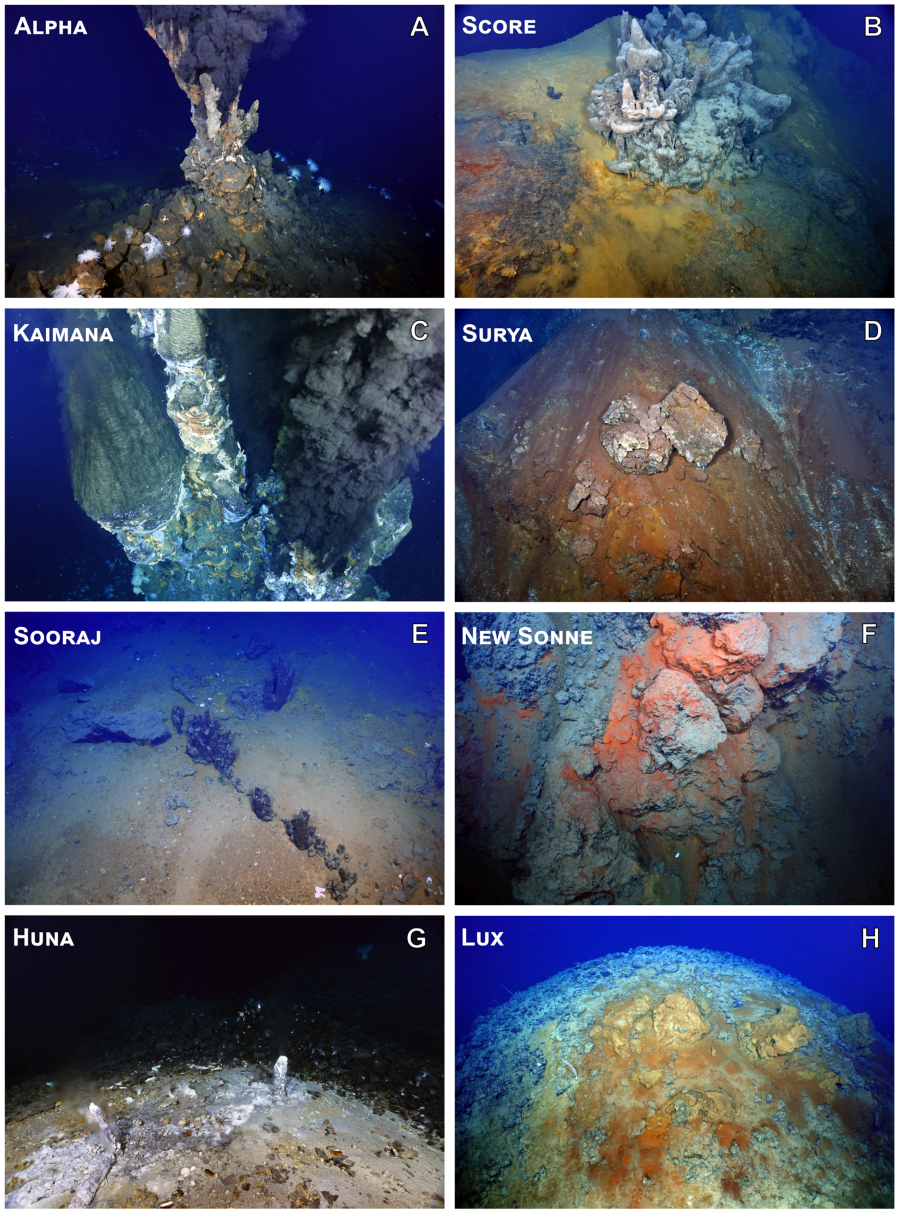


Figure 3

Selected seafloor images of eight newly discovered vent fields and SMS occurrences along the southern Central Indian Ridge (A–C) and the northern Southeast Indian Ridge (D–H). The images illustrate the diversity of hydrothermal precipitates and mound morphologies observed in the different vent fields, ranging from active black smokers (A), large mature black smoker complexes with beehive spires and typical vent fauna (C), and inactive but intact chimneys (B), to waning-stage low-temperature venting (D), late-stage weathering and sulfide oxidation (F, H), fissure- and fault-controlled chimney occurrences at Sooraj (E), and silica precipitation at Huna (G).

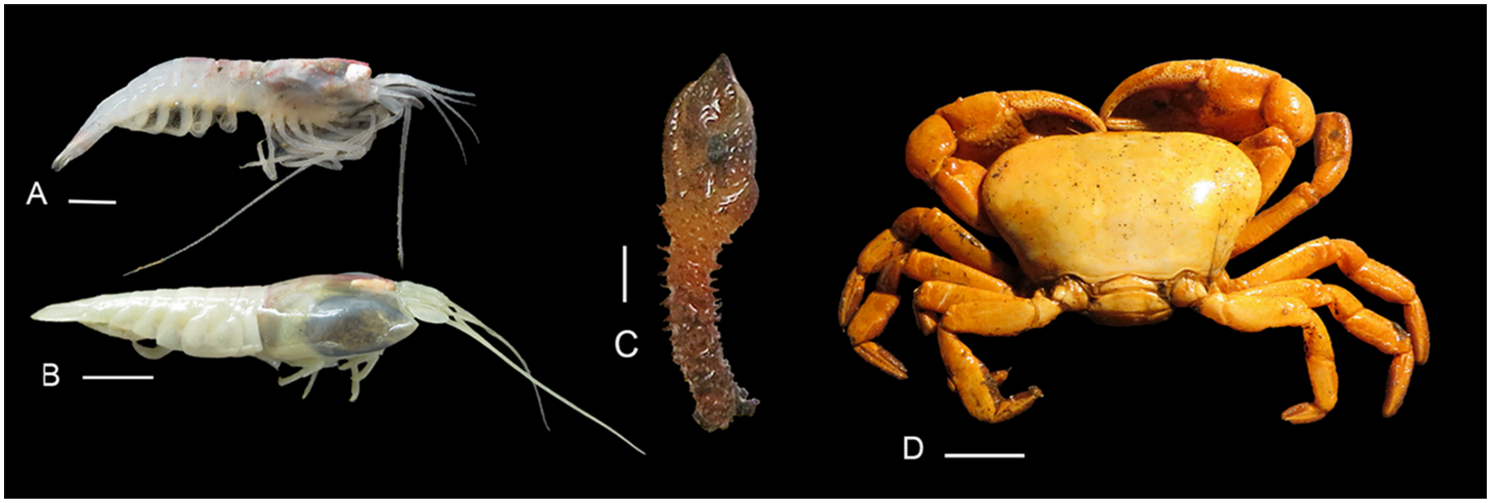


Figure 4

Photographs of selected crustaceans from different vent fields. A: *Mirocaris indica*; B: *Rimicaris kairei*; C: *Neolepas marisindica*; D: *Austinograea rodriguezensis*. Scale bars: 1 cm.

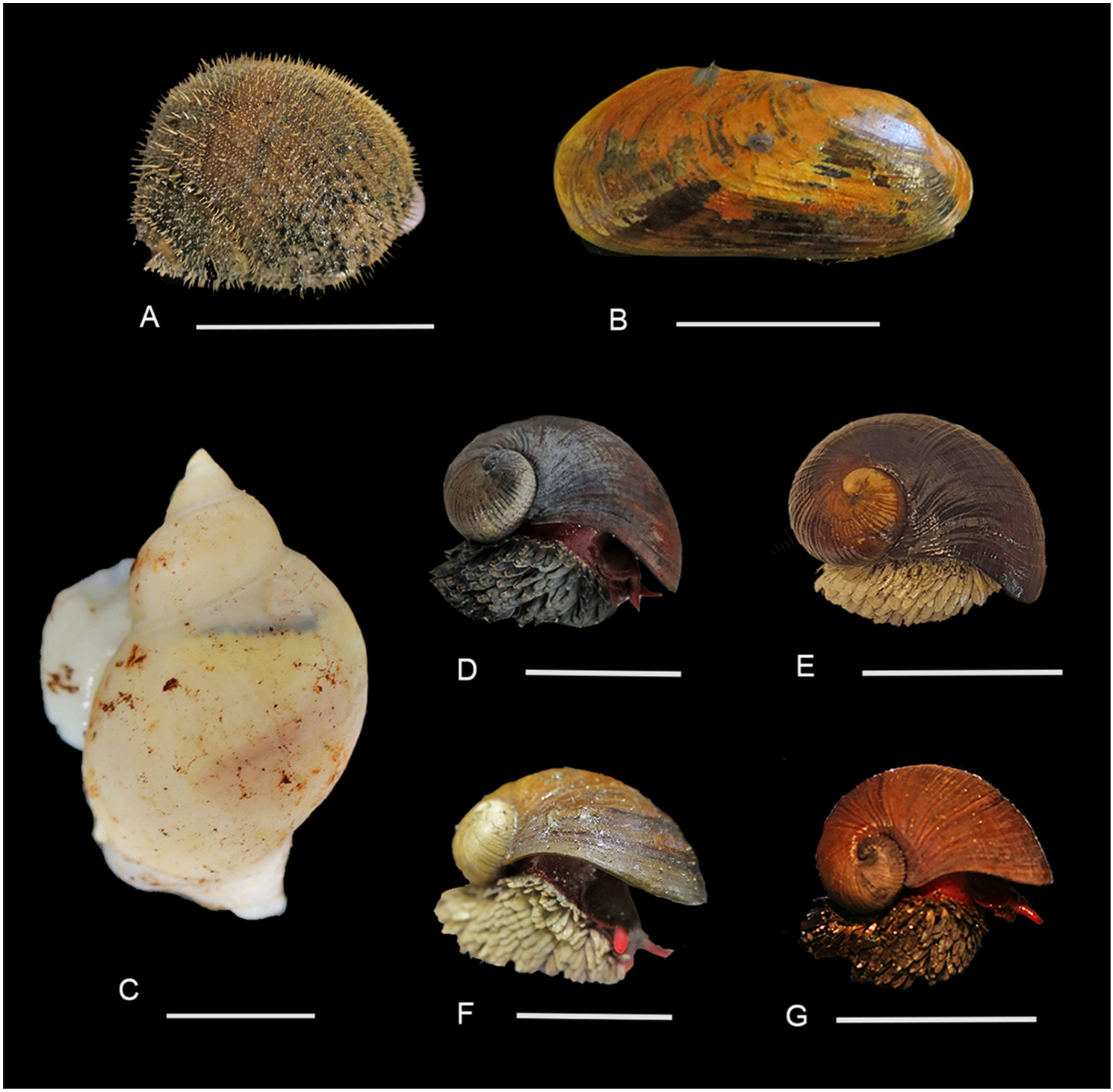


Figure 5

Photographs of selected molluscs from different vent fields. A: *Alviniconcha marisindica*; B: *Bathymodiolus septemdierum*; C: *Phymorhynchus* sp.; D–G: different morphotypes of *Chrysomallon squamiferum*. Scale bars: 3 cm.

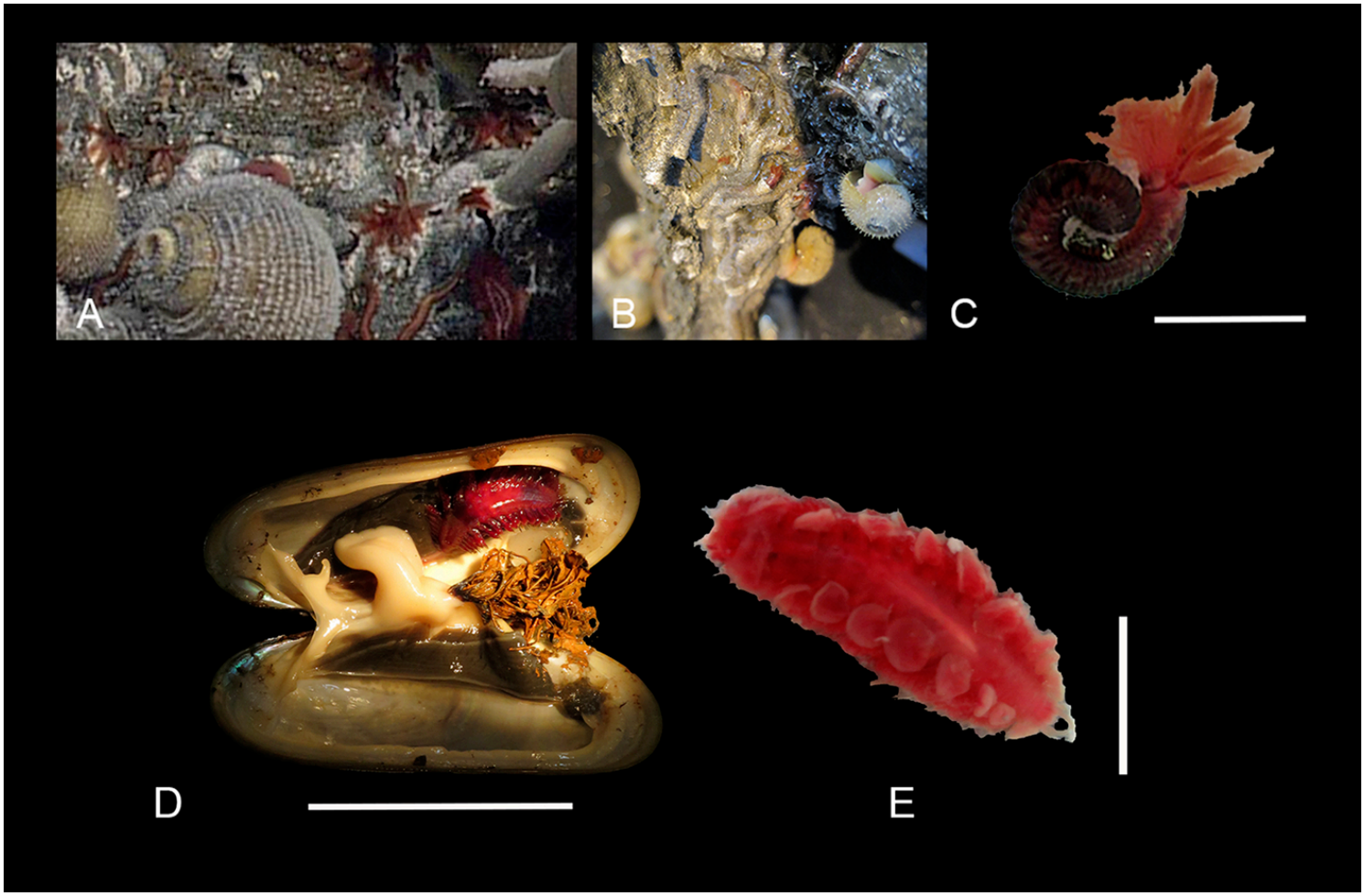


Figure 6

Photographs of selected polychaetes from different vent fields. A–C: *Paralvinella mira*; D: *Bathymodiolus septemdierum* hosting *Branchipolynoe longqiensis*; E: *Branchipolynoe longqiensis*. Scale bars: C = 1 cm, D = 5 cm, E = 1.5 cm.

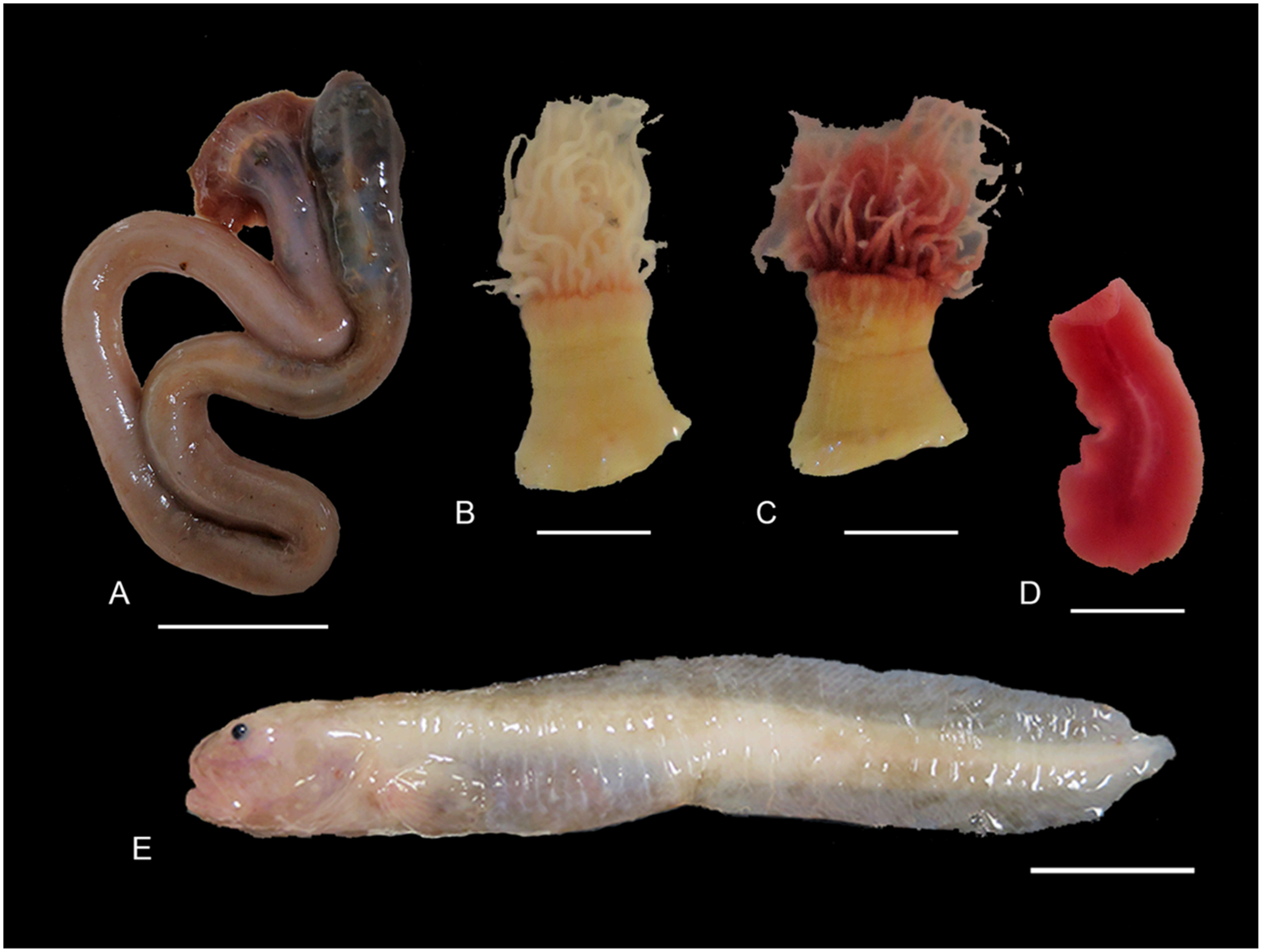


Figure 7

Photographs of selected taxa from different vent fields. A: *Chiridota* sp.; B–C: *Maractis*sp.; D: Polycladida sp.; E: *Pachycara angeloi*. Scale bars: A = 2 cm, B–C = 3 cm, D = 1 cm, E = 3.5 cm.

Image not available with this version

Figure 8

Faunal zonation along an active hydrothermal vent. A: active vent site with venting chimney; B: vent orifices with aggregations of *Rimicaris kairei*; C: clusters of *Alviniconcha marisindica* and *Chrysomallon squamiferum*with *Austinograea rodriguezensis* and *Phymorhynchus* spp.; D: *Bathymodiolus septemdierum* with few individuals of *Phymorhynchus* spp.; E: peripheral zone with *Maractis* spp. and *Phymorhynchus* spp.

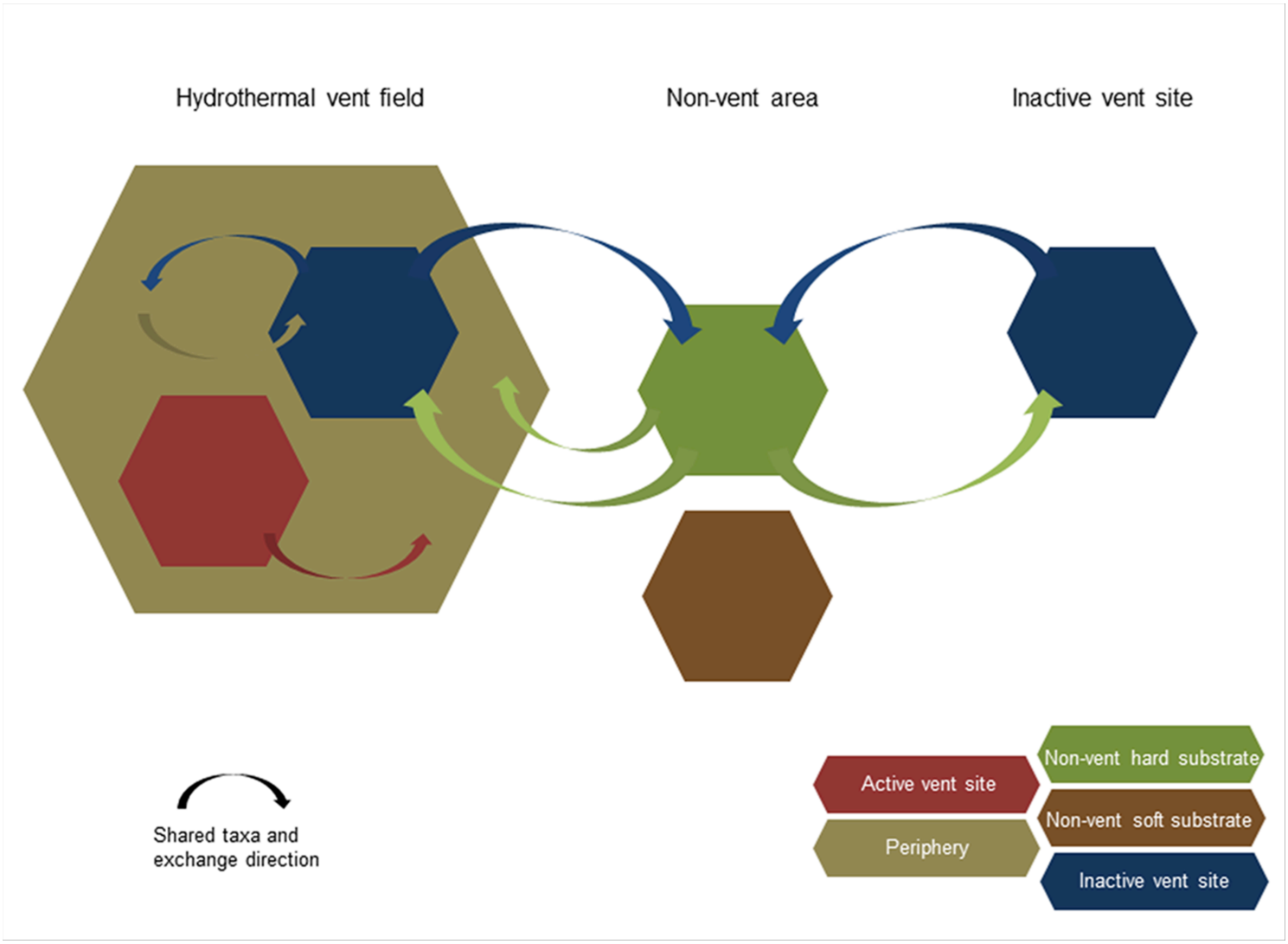


Figure 9

Schematic representation of shared taxa and faunal exchange among active vent sites, inactive SMS sites, and non-vent areas.

Supplementary Files

This is a list of supplementary files associated with this preprint. Click to download.

- STable6NonVent.xlsx
- STable4Inactive.xlsx
- STable5Peripher.xlsx
- STable1GeologicalCharacteristics.xlsx
- STable3Diffuse.xlsx
- STable2Active.xlsx
- STable7MetadataStations.xlsx
- SFigures114ventfields.pdf